



HAL
open science

Optimization of the Pechini-derived synthesis of rare-earth free aluminum borate phosphors presenting tunable white emission

Jérémy Cathalan, Mathieu Salaün, Pierre Gaffuri, Audrey Potdevin, François Réveret, Alain Ibanez, Geneviève Chadeyron, Isabelle Gautier-Luneau

► To cite this version:

Jérémy Cathalan, Mathieu Salaün, Pierre Gaffuri, Audrey Potdevin, François Réveret, et al.. Optimization of the Pechini-derived synthesis of rare-earth free aluminum borate phosphors presenting tunable white emission. *Journal of Materials Science*, 2022, 57, pp.15829-15842. 10.1007/s10853-022-07619-5 . hal-03761518

HAL Id: hal-03761518

<https://hal.science/hal-03761518>

Submitted on 26 Aug 2022

HAL is a multi-disciplinary open access archive for the deposit and dissemination of scientific research documents, whether they are published or not. The documents may come from teaching and research institutions in France or abroad, or from public or private research centers.

L'archive ouverte pluridisciplinaire **HAL**, est destinée au dépôt et à la diffusion de documents scientifiques de niveau recherche, publiés ou non, émanant des établissements d'enseignement et de recherche français ou étrangers, des laboratoires publics ou privés.



Optimization of the Pechini-derived synthesis of rare-earth free aluminum borate phosphors presenting tunable white emission

Jérémy Cathalan^{1,2}, Mathieu Salaün^{1,*} , Pierre Gaffuri¹ , Audrey Potdevin² , François Réveret² , Alain Ibanez¹, Geneviève Chadeyron² , and Isabelle Gautier-Luneau^{1,*}

¹Univ. Grenoble Alpes, CNRS, Grenoble INP, Institut Néel, 38000 Grenoble, France

²Université Clermont Auvergne, Clermont Auvergne INP, CNRS, Institut de Chimie de Clermont-Ferrand, 63000 Clermont-Ferrand, France

Received: 4 June 2022

Accepted: 7 August 2022

© The Author(s), under exclusive licence to Springer Science+Business Media, LLC, part of Springer Nature 2022

ABSTRACT

The present study is dedicated to the development of aluminum borate luminescent powders which appear as promising and more environmental-friendly than conventional phosphors. The different steps of the luminescent powder synthesis, in particular the precursors (inorganic and organic) ratios and calcination conditions, are adjusted by studying the resulting optical features to get a broader and warmer white emission. As shown in previous works, the photoluminescence emission originates from polyaromatic hydrocarbons trapped in the inorganic aluminum borate matrix. Morphological and structural properties of the particles remain otherwise identical for every optimized parameter. The aluminum borate powder synthesized in these optimized conditions exhibits a wide and intense emission band under near-UV excitation. These structural and optical properties combined with time-resolved photoluminescence measurements demonstrate that the adjustments of the synthetic process allow the formation and trapping of more and different emitting centers. The modulation of the excitation wavelength (from 305 to 405 nm) leads to a tunable photoluminescence emission characterized by a large band lying between 400 and 700 nm. This feature, associated with the use of secure and abundant precursors makes aluminum borate powders very interesting phosphors for optical applications.

Handling Editor: Till Froemling.

Address correspondence to E-mail: mathieu.salaun@neel.cnrs.fr; Isabelle.Gautier-Luneau@neel.cnrs.fr

<https://doi.org/10.1007/s10853-022-07619-5>

Springer

	Journal : 10853 - Large 10853	Dispatch : 21-8-2022	Pages : 14
	Article No. : 7619	<input type="checkbox"/> LE	<input type="checkbox"/> TYPESET
	MS Code : JM5C-D-22-03115R1	<input checked="" type="checkbox"/> CP	<input checked="" type="checkbox"/> DISK

44 **Introduction**

45
46 Solid-state white light displays using light emitting
47 diodes (LEDs) have emerged over the last decade and
48 they are substituting traditional technologies thanks
49 to a significantly reduced energy consumption. The
50 phosphor-converted (pc)-White LEDs (WLEDs) usu-
51 ally combine a semiconductor chip emitting in the
52 ultraviolet or blue wavelength range to one or more
53 phosphor(s) generally deposited in the form of coat-
54 ings using either on-chip or remote configurations
55 [1]. Herein, we will focus on the last one.

56 Commonly commercialized pc-WLEDs are com-
57 posed of a blue-emitting InGaN LED covered by a
58 composite material made of a polymeric matrix in
59 which a mixture of luminescent compounds is dis-
60 persed: the yellow phosphor cerium-doped yttrium
61 aluminum garnet ($\text{Y}_3\text{Al}_5\text{O}_{12}:\text{Ce}^{3+}$ or YAG:Ce) [2–4]
62 usually blended with a red phosphor (generally Eu^{2+}
63 doped nitride or sulfide compounds) to convert the
64 chip emission into a warm white emission [5–7].

65 More recently, the use of near-UV LEDs as excita-
66 tion sources has attracted a lot of attention in order to
67 optimize photometric parameters such as color render-
68 ing index (CRI) or correlated color temperature
69 (CCT). Several strategies are exposed in the literature:
70 the most common consists in the association of the
71 UV LED with red, green and blue (RGB) phosphors
72 to generate an overall white light. Two approaches
73 for the mixture of colors are then considered. The first
74 one involves the mixture of the three RGB phosphors
75 to prepare a one-layer coating with a broad emission
76 band covering the entire visible spectrum [8, 9]. The
77 second process is based on the superposition of three
78 layers of single-color phosphors: phosphor powder
79 dispersed in a polymeric matrix or phosphor in glass.
80 Major issues of cascade-excitation resulting in a low
81 luminous efficacy are raised [8, 10], an important
82 optimization work has to be done to reduce this
83 phenomenon. Another way to obtain white light
84 using UV LED is to combine it with a suitably doped
85 (Eu^{2+} , Eu^{3+} , Dy^{3+}) or co-doped ($\text{Tm}^{3+}/\text{Tb}^{3+}/\text{Eu}^{3+}$,
86 $\text{Tm}^{3+}/\text{Dy}^{3+}$, $\text{Yb}^{3+}/\text{Er}^{3+}/\text{Tm}^{3+}$) single-phase host
87 such as silicates, phosphates or even oxychlorides
88 [11].

89 Both blue- and UV-excitation systems aforemen-
90 tioned lift two main drawbacks: an instability of their
91 photometric parameters due to temperature aging
92 and the use of rare-earths (RE) in phosphors

composition (yttrium, cerium, europium...) 93
[4, 12–14]. These latter have been classified as critical 94
elements by the European Union [15]. The ore 95
extraction requires important quantities of chemicals, 96
water and energy [16, 17], and it is thus associated 97
with environmental and economic issues [17–19]. 98
Most of the generated pollution results from the 99
storage of the residues from the ore refining. The 100
wastewaters and processed chemicals are stored in 101
huge open air retention basins. Among these toxic 102
spills, we can cite heavy metals and radioactive ele- 103
ments: soil, air and surface/groundwater can be 104
contaminated in large areas around the mines 105
[20–22]. Hence, developing alternative phosphors to 106
overcome these issues is getting increasing attention. 107

108 A first step to reduce the RE quantity in the pc-
109 WLED devices is to combine YAG:Ce with a RE-free
110 red phosphor. Manganese ions ($\text{Mn}^{2+}/\text{Mn}^{4+}$) are
111 promising candidates thanks to their photolumines-
112 cence (PL) properties in the red wavelength range
113 [23, 24]. For example, Mn^{4+} -doped fluoride K_2SiF_6
114 (KSF) host matrix, allowing a red emission without
115 the use of RE, has been developed by several pro-
116 cesses. However, moisture stability and control of the
117 oxidation degree of manganese should be improved
118 though [25].

119 Quantum dots (QDs) [26] and often more specifi-
120 cally carbon dots (CDs) [27–29] are other promising
121 RE-free materials owing to their narrow PL emission
122 band adjustable over the full visible spectrum thanks
123 to the possible mixing of several different color
124 emitting QDs. Thus, QDs show good potential for
125 white LED phosphors application [30–32]. Never-
126 theless, they present low quantum yields (QYs) in the
127 solid state and their UV/thermal stability remains
128 unsuitable for commercial requirement for the time
129 being.

130 Among possible RE-free phosphors, one can also
131 find silica-based luminescent materials such as sili-
132 cate-carboxylate, silica nanowires and aluminum sil-
133 icate [33–35]. The decomposition of organic
134 precursors during synthesis or post-synthesis ther-
135 mal treatments leads to carbon, carbonyl or hydro-
136 carbon defects to which the luminescence is
137 attributed. The same phenomenon has been proposed
138 for yttrium aluminum borate (YAB) synthesized by
139 the modified Pechini process [36]. More recently, for
140 YAB powders prepared by a sol-gel process, we
141 evidenced by involving complementary techniques
142 as ^{13}C labeling nuclear magnetic resonance (NMR)

143 and electron paramagnetic resonance (EPR) spectro-
 144 scopies, thermal analyses, optical properties and DFT
 145 calculations, that the PL emission originates from
 146 polyaromatic hydrocarbon (PAH) molecules entrap-
 147 ped in the inorganic matrix [37–39]. In the same way,
 148 larger extended polyaromatic molecules (seven rings
 149 and more) with hydroxyl or other oxygenated groups
 150 have been proposed as PL emitting centers produced
 151 during the successive thermal treatments (pyrolysis
 152 and calcination) in the case of modified Pechini-syn-
 153 thesized YAB [40]. Subsequently, the necessity to
 154 replace critical elements (yttrium here) from the
 155 material composition has led to the study of zinc
 156 aluminum borate (ZAB) where not only the glassy
 157 network modifier was changed but also the glassy
 158 matrix forming elements (aluminum and boron) ratio
 159 has been optimized to improve the trapping of the PL
 160 emitting centers [41]. Even if borates are known as
 161 very interesting optical materials, as highlighted in
 162 the recent review [42], their study as rare-earth-free
 163 phosphors is rather new and concerns not necessarily
 164 crystallized borate matrices.

165 In this paper, based on our previous results, we
 166 eliminate the glass modifier (zinc) from the compo-
 167 sition and we describe the development of a rare-
 168 earth free phosphor: a luminescent aluminum borate
 169 (AB) micrometric powder with a $Al_xB_yO_z$ general
 170 formula. The structural and morphological charac-
 171 teristics of this powder have been studied by powder
 172 X-ray diffraction (PXRD) and scanning and trans-
 173 mission electron microscopies (SEM—TEM). The
 174 stoichiometric precursors ratios used for the synthe-
 175 ses leading to AB powders with the best lumines-
 176 cence properties in terms of PL emission profile and
 177 intensity have been determined thanks to optical
 178 studies. These latter have been carried out using a
 179 near-UV excitation source similar to commercial UV
 180 LED chips. Once the precursors ratio optimized, the
 181 heating treatment conditions leading to the most
 182 suitable AB powder optical properties have been
 183 identified. The optical properties have been charac-
 184 terized by recording emission spectra using different
 185 excitation wavelengths and performing time-re-
 186 solved photoluminescence spectroscopy measure-
 187 ments (TRPL).

Experimental 188

Materials 189

Citric acid monohydrate was purchased from Sigma-
 190 Aldrich (purity 99.0 + %). aluminum nitrate
 191 $Al(NO_3)_3 \cdot 9H_2O$ (purity 99.0 + %), D-sorbitol (purity
 192 97.0 + %), boric acid H_3BO_3 (purity 99.8%) and
 193 ultrapure water (0.63 $\mu S/cm$) were purchased from
 194 Fisher Scientific. 195

Synthesis of AB powder by modified Pechini method 196

The synthesis of AB luminescent powders has been
 198 conducted following the modified Pechini method
 199 similar to that already described [41, 43]. Based on
 200 these previous works, Fig. 1 illustrates the different
 201 preparation steps. Citric acid monohydrate (Cit: 35 to
 202 100.8 mmol) and $Al(NO_3)_3 \cdot 9H_2O$ amounts (Al: 4.2 to
 203 9 mmol) are dissolved in 50 mL of ultrapure water at
 204 80 °C under stirring for 20 min (solution 1). At the
 205 same time, D-sorbitol (Sorb: 33.6 to 70 mmol) and
 206 H_3BO_3 amounts (B: 12 to 16.8 mmol) are dissolved in
 207 the same conditions (solution 2). The powder PL has
 208 been optimized by exploring different molar ratios
 209 among precursors: the inorganic ratio, $R_i = Al/B$, the
 210 organic ratio, $R_o = Cit/Sorb$, and the organic/inor-
 211 ganic ratio, $R_{o/i} = (Cit + Sorb)/(Al + B)$. R_i has been
 212 studied from 0.25 to 0.75, R_o from 0.5 to 2 and $R_{o/i}$
 213 from 4 to 8. All the ratios are summarized in Table 1.
 214

Solution 1 and solution 2 were mixed together and
 215 heated under reflux at 100 °C for 48 h (first step,
 216 Fig. 1) leading to a yellowish/orange color solution.
 217 This resulting solution was partially evaporated at
 218 80 °C in a ventilated furnace, initiating the
 219 polyesterification reactions and subsequently heated
 220 at 250 °C for 30 min with a heating rate of 30 °C/h
 221 under air. An expanded brown solid was obtained
 222 and crushed 5 times by dry planetary milling for
 223 3 min at 430 rpm in a zirconia bowl with 0.5 mm
 224 diameter zirconia balls with an air/powder/bead
 225 ratio of 1/1/1 by volume (second step, Fig. 1). The
 226 fine brown powder was pyrolyzed at 700 °C for 12 h
 227 with a HR of 30 °C/h under a continuous N_2 flow
 228 (approx. 10 mL/min). These conditions lead to
 229 eliminate a large part of organics (69% mass loss
 230 measured by thermogravimetric analysis (TGA),
 231 Figure S1) without hot spots that could induce
 232 inhomogeneities. The black powder resulting from
 233

234 the pyrolysis was sieved to select grains with a
 235 diameter smaller than 25 μm . The final thermal
 236 treatment was a calcination under a continuous O_2
 237 flow of 10 mL/min. For a further study, heating rate
 238 (HR) and calcination temperature (T_{ca}) were investi-
 239 gated from 20 $^\circ\text{C}/\text{h}$ to 90 $^\circ\text{C}/\text{h}$ and from 680 $^\circ\text{C}$ to
 240 720 $^\circ\text{C}$, with a dwell time of 10 min, respectively.
 241 During this step, a large part of the remaining organic
 242 moieties was oxidized leading to 77% mass loss
 243 mainly through CO_2 and H_2O (Figure S2). The total
 244 mass loss during the thermal treatments (pyrolysis
 245 + calcination) reaches 93%. The final powder is
 246 beige and luminescent under UV excitation. The
 247 thermal treatments conditions presented in Fig. 1
 248 were set according to the study of ZAB powders
 249 carried out by Gaffuri et al.[41]. The luminescent AB
 250 powder was synthesized at first in these reported
 251 conditions and will be subsequently referred as
 252 "reference sample."

253 Characterizations

254 Microstructural properties

255 **Powder X-ray diffraction** PXRD patterns of AB pow-
 256 ders were recorded using a Bruker D8 Endeavor
 257 diffractometer operating with $\text{Cu-K}\alpha$ radiation
 258 ($\lambda = 1.5418 \text{ \AA}$) with a goniometer in a symmetrical
 259 geometry. The data were collected in a 2θ range with
 260 a scan speed of $1^\circ/\text{min}$.

261 **Thermogravimetric analysis coupled mass spectrometry** Differential thermal analysis (DTA), and TGA

Table 1 Molar ratios of the precursors, aluminum nitrate, boric acid, citric acid and D-sorbitol used for the preparation of the different samples. **a** study of influence R_o ratio with $R_{o/i} = 5$ **b** study of influence of $R_{o/i}$ ratio with $R_o = 1.5$

(a)	(R_o)	Al	:	B	:	Cit	:	Sorb
	0.5	1	:	2	:	5	:	10
	0.75	1	:	2	:	6.4	:	8.6
	1	1	:	2	:	7.5	:	7.5
	1.25	1	:	2	:	8.3	:	6.7
	1.5*	1	:	2	:	9	:	6
	2	1	:	2	:	10	:	5
(b)	($R_{o/i}$)	Al	:	B	:	Cit	:	Sorb
	4	1	:	2	:	7.2	:	4.8
	5*	1	:	2	:	9	:	6
	6	1	:	2	:	10.8	:	7.2
	6.5	1	:	2	:	11.7	:	7.8
	7	1	:	2	:	12.6	:	8.4
	8	1	:	2	:	14.4	:	9.6

*Reference sample: molar ratio for Cit and Sorb used for YAB and ZAB powders.

263 were carried out with a SETARAM TAG 16 equip-
 264 ment, using 30 mg samples within 100 μL alumina
 265 crucibles and a heating rate of 5 $^\circ\text{C}/\text{min}$ under pure
 266 (Airproducts, alphagaz 2) oxygen. These thermal
 267 analyses were directly coupled to a HIDEN analytical
 268 apparatus (QGA-HAL201-RC) mass spectrometer to
 269 analyze the gaseous by-products of decompositions.

270 **Granulometry** Grain sizes of powders were mea-
 271 sured by laser granulometry with a Malvern

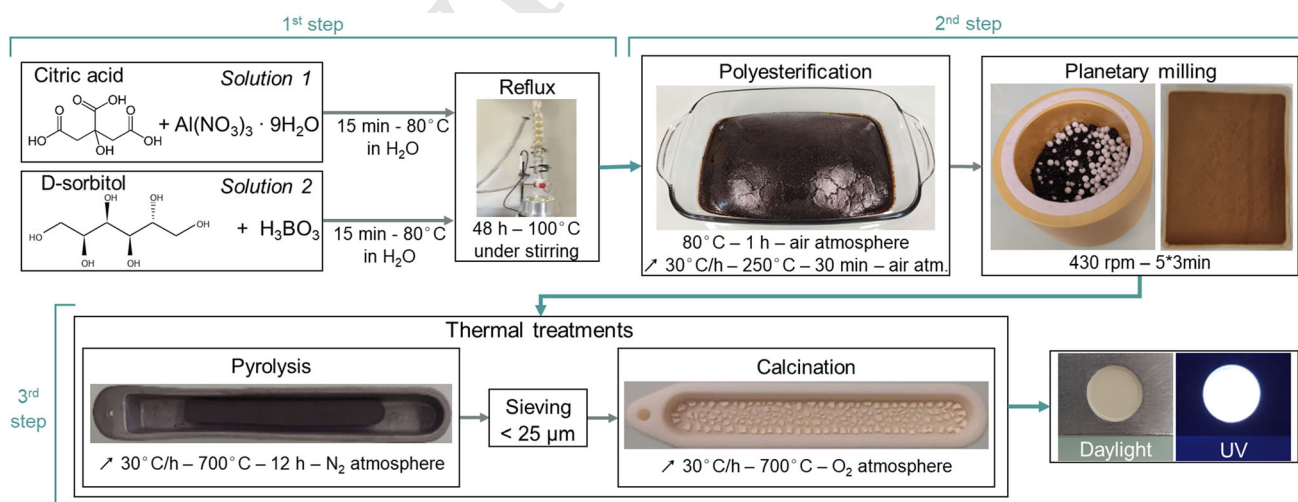


Figure 1 Modified Pechini synthesis of aluminum borate luminescent powders in three major steps.

272 Mastersizer 2000. Dispersing agent was absolute
273 ethanol.

274 **Microscopy** The powder particles have been
275 observed in a field emission scanning electron
276 microscope (FESEM) ZEISS Ultra + . Acceleration
277 voltage $V = 2.0$ kV & $V = 4.0$ kV.

278 Transmission Electronic Microscopy (TEM) images
279 were recorded on a Hitachi H-7650 microscope at the
280 Centre Imagerie Cellulaire Santé (CICS) of Clermont-
281 Ferrand. Acceleration voltage $V = 80$ kV.

282 **Optical properties Quantum yields & photoluminescence**
283 **emission** QY efficiencies and emission spectra of the
284 powders were measured using a C9920-02G PLQY
285 integrating sphere measurement system from
286 Hamamatsu Photonics. The setup consisted of a
287 150 W monochromatized Xe lamp, an integrating
288 sphere (Spectralon coating , diameter = 3.3 in) and a
289 high-sensitivity CCD camera. All measurements
290 were carried out at room temperature.

291 External quantum yield (eQY) was calculated from
292 the internal quantum yield (iQY) and absorption
293 coefficient (Abs) measurements according to Eq. (1):

$$294 \quad eQY = iQY \times Abs \quad (1)$$

295 Measurement uncertainties of iQY and Abs are 5%
296 of the measured values, eQY uncertainty arises from:

$$297 \quad \frac{\Delta eQY}{eQY} = \frac{\Delta iQY}{iQY} + \frac{\Delta Abs}{Abs} \quad (2.1)$$

$$300 \quad \Delta eQY = \Delta iQY \times Abs + \Delta Abs \times iQY \quad (2.2)$$

$$302 \quad \Delta eQY = 5\% \times iQY \times Abs + 5\% \times Abs \times iQY \quad (2.3)$$

$$304 \quad \Delta eQY = 10\% \times eQY \quad (2.4)$$

306

307 **Time-resolved photoluminescence** TRPL was per-
308 formed at room temperature. The excitation source
309 was the second harmonic (400 nm) of a Ti:Sa pulsed
310 laser with a pulse duration of 150 fs and a repetition
311 rate of 76 MHz. The average power on the sample is
312 equal to 5 W cm^{-2} . The photoluminescence signal
313 was collected in a 32 cm focal monochromator using
314 a grating with 300 gr/mm coupled with a streak
315 camera.

Results and discussion

316

As noticed in the introduction, Burner et al. identified
317 carbonaceous species, PAHs-type small molecules, as
318 emitting centers of the sol-gel-synthesized YAB
319 powders [37]. The presence of larger PAH molecules
320 as emitting centers was recently confirmed for YAB
321 powders synthesized by the modified Pechini
322 method [40]. Based on this knowledge, we selected
323 several synthesis parameters that seemed relevant to
324 favor the formation of PAH-like molecules trapped in
325 the inorganic matrix to improve the photometric
326 parameters of the AB powders. Therefore, the influ-
327 ence of molar ratios of the different inorganic and
328 organic precursors, as well as the calcination condi-
329 tions (heating rate and temperature of calcination)
330 were studied. Before presenting the optimization of
331 these parameters using the optical study, the first
332 part of this section will be dedicated to structural and
333 morphological properties of AB powders, that remain
334 identical whatever the precursor ratios. 335

Grain morphology and structure

336

SEM images of the typical AB sample were recorded
337 after each synthesis step and are presented with the
338 corresponding PXRD patterns in Fig. 2 to study its
339 structure-morphology relationship. The brown
340 expanded matrix milled in a micron-sized powder
341 has a slight porosity due to the off-gassing occurring
342 during polyesterification reactions (Fig. 2a). On the
343 PXRD pattern (Fig. 2a), a weak peak at $2\theta = 28^\circ$ (in-
344 dexed by a red up-triangle) is attributed to H_3BO_3
345 recrystallization. The PXRD pattern of the pyrolyzed
346 powder (Fig. 2b) reveals a totally amorphous materi-
347 al. The SEM images show rough faces and smoother
348 ones, marked by conchoidal fractures (highlighted on
349 the 300-nm-scaled photograph, Fig. 2b), specific to
350 glassy materials. The SEM photograph 3- μm -scaled
351 of AB powder calcined at 700°C (Fig. 2c) evidences a
352 similar aspect to the pyrolyzed one. The luminescent
353 powder keeps the glassy characteristics evidenced by
354 the conchoidal fractures. Furthermore, some grains
355 present on their surface a thin crust of 10 nm-diam-
356 eter nanowires (weak surface crystallization,
357 Fig. 2c—confirmed by TEM study, Figure S3)
358 assigned to the $\text{Al}_4\text{B}_2\text{O}_9$ phase according to the cor-
359 responding PXRD pattern (Fig. 2c) [41]. On the other
360 hand, the H_3BO_3 partial recrystallization is indicated
361 by the presence of the thin intense peak at 28° (2θ). 362

363 This phenomenon may be due to the hydrolysis of
 364 the boron in the matrix. The grain size was controlled
 365 thanks to the sieving step before calcination and
 366 measured by laser granulometry both after pyrolysis
 367 (volume-weighted mean diameter, denoted
 368 $D_{4,3} = 18 \mu\text{m}$) and calcination ($D_{4,3} = 9 \mu\text{m}$) steps
 369 (Figure S4). In the following investigations, all powders
 370 were assumed to be with similar morphology
 371 and granulometry.

372 Optimization of the inorganic ratio R_i

373 The network modifiers (Y^{3+} or Zn^{2+} cations) have
 374 been removed from the glassy inorganic matrix in
 375 this study. Thus, it is important to check the ability of
 376 the AB matrix to trap PAH emitting centers. The
 377 influence of the Al/B molar ratio was studied starting
 378 from the previous results obtained for ZAB powders
 379 [41]. Three samples were prepared as described in the
 380 experimental section ($R_i = 0.25; 0.5; 0.75$). Their opti-
 381 cal properties have been studied. The eQY of samples
 382 calcined at $650 \text{ }^\circ\text{C}$, $675 \text{ }^\circ\text{C}$, $700 \text{ }^\circ\text{C}$ and $725 \text{ }^\circ\text{C}$
 383 was measured for an excitation wavelength of

$\lambda_{\text{exc}} = 385 \text{ nm}$ (Figure S5). The highest eQY
 384 ($17.9\% \pm 1.8\%$) was reached for a $R_i = 0.5$ calcined at
 385 $700 \text{ }^\circ\text{C}$. This ratio is associated with a broader and
 386 more intense PL emission band than the 0.25 and 0.75
 387 Al/B ratios for the same calcination temperature
 388 (Figure S6). Thus, as observed for ZAB matrices,
 389 samples with R_i larger than 0.75 were characterized
 390 by colder PL emissions and lower eQYs. This con-
 391 firms that the inorganic precursors ratio affects the
 392 formation and trapping mechanisms of the PAH
 393 molecules by the aluminum borate matrices. There-
 394 fore, the Al/B ratio of 0.5 was selected for the fol-
 395 lowing optimization studies.
 396

397 Optimization of R_o and $R_{o/i}$ molar ratios

398 Organic precursors being at the origin of the forma-
 399 tion of PAH molecules within the inorganic matrix,
 400 the influence of R_o and $R_{o/i}$ ratios on the PL of
 401 powders was studied. On one hand, the R_o ratio
 402 assesses the importance of both precursors, citric acid
 403 (α -hydroxylated tricarboxylic acid) and sorbitol
 404 ($\text{C}_6\text{H}_8(\text{OH})_6$) which play the role of complexing

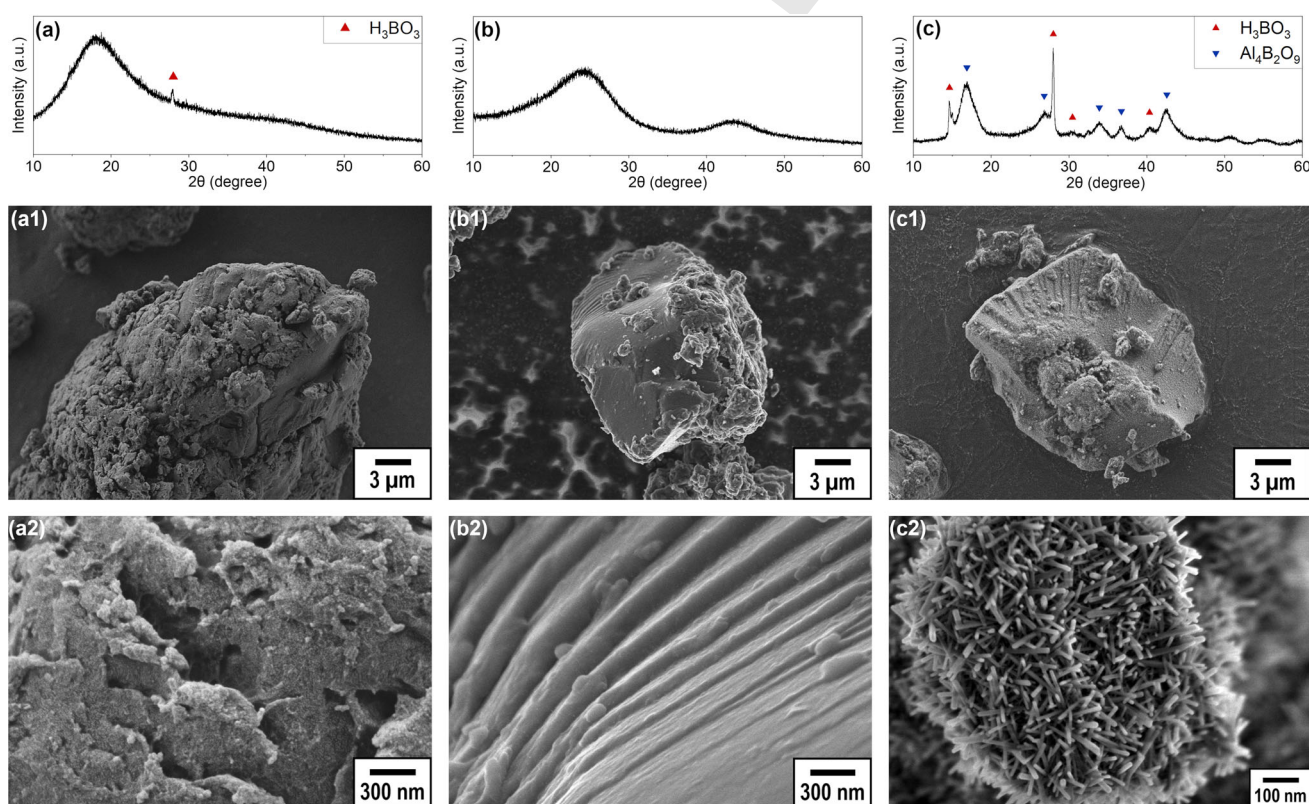


Figure 2 XRD patterns and corresponding SEM images of AB sample after each step of the modified Pechini synthesis: **a a1 a2** brown powder, **b b1 b2** powder pyrolyzed at $700 \text{ }^\circ\text{C}$, **c c1 c2** powder calcined at $700 \text{ }^\circ\text{C}$.

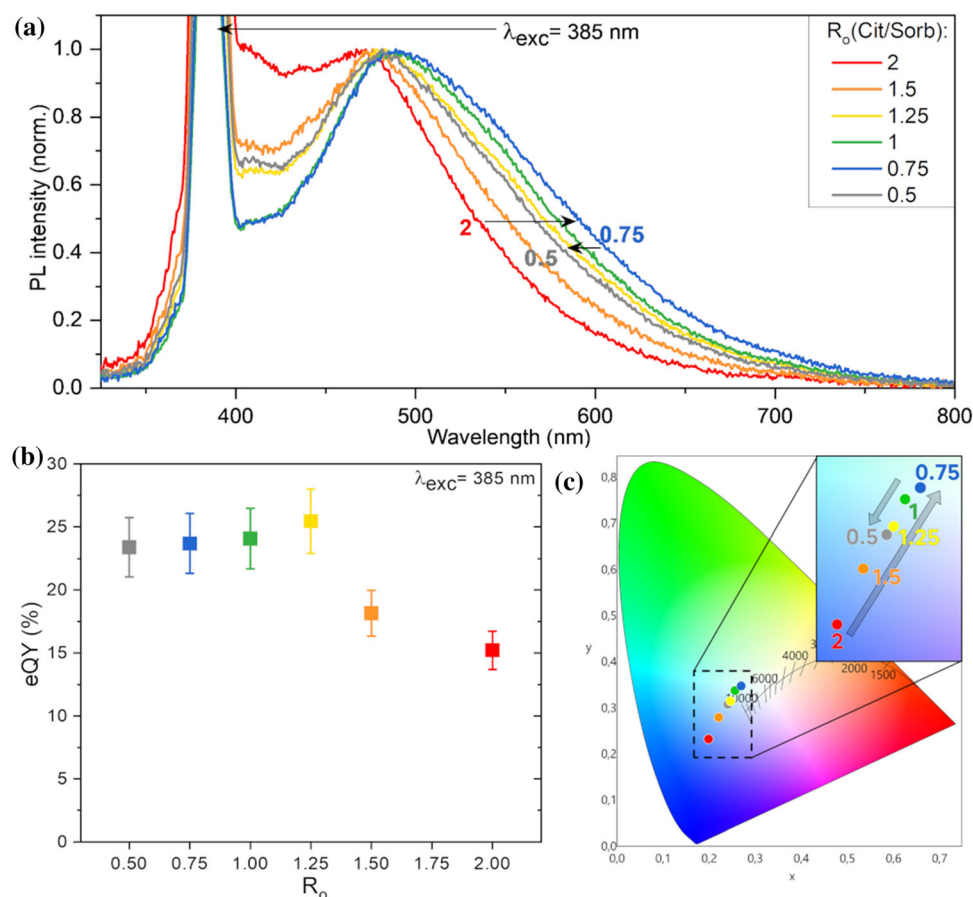


Figure 3 Normalized PL emission spectra (a) and corresponding eQYs (b) and CIE (Conference Internationale de l'Eclairage 1931) chromaticity coordinates (c) of AB samples with R_o ratios varying from 0.5 to 2.

agents of aluminum and boron atoms and allow the formation of the polymer network by esterification between free carboxylic and alcohol functions. On the other hand, the $R_{o/i}$ ratio was adjusted keeping R_o constant in order to evaluate the best quantity of organic compounds to use relative to aluminum and boron forming the inorganic network. The different compositions have been compared with the results obtained for the initial synthesized powder considered as reference. The investigated R_o and $R_{o/i}$ ratios varied from 0.5 to 2 for R_o and from 4 to 8 for $R_{o/i}$ with R_i kept constant at 0.5 (Table 1). The PL properties (emission spectra and QY) of all these samples have been studied to select the ratio leading to the best photometric characteristics.

Figure 3 presents the normalized PL emission spectra of samples with R_o varying from 0.5 to 2 for a fixed $R_{o/i} = 5$ (reference value, Table 1). The near-UV excitation wavelength has been set to 385 nm since it

corresponds to the wavelength of some commercial UV LEDs. The PL emission spectrum of the reference sample ($R_o = 1.5$, in orange) has a broad emission band lying from the blue to the yellow wavelengths range. Decreasing the R_o from 2 to 0.75 progressively shifts and widens the PL emission spectra to higher emission wavelengths (Fig. 3a). This is confirmed by the CIE chromaticity coordinates: the emission is warmer when R_o decreases from 2 to 0.75 (Fig. 3c). With a lower $R_o = 0.5$, the PL emission goes backward to a colder color. Corresponding eQYs for the same excitation wavelength (385 nm) are shown in Fig. 3b. The maximum value of the eQY (25.4% \pm 2.5%) is obtained for $R_o = 1.25$. Below this R_o , eQY remains between 23.4% \pm 2.3% and 24.1% \pm 2.4%. Above this ratio, the eQY decreases to 15.2% \pm 1.5%.

In addition, during syntheses, we noticed that R_o below 1 led to the formation of poorly expanded

443 brown solids with a higher hardness making the
 444 grinding and sieving steps more difficult. Thus, the
 445 grain size is less controllable. In fact, a low R_o reduces
 446 the CO_2 off-gassing resulting from the decarboxylation
 447 of the citrate during the heating of the
 448 polyesterification step. In conclusion, the $R_o = 1$
 449 seems to be a good compromise to keep an easy-to-
 450 grind powder presenting suitable optical properties:
 451 an eQY of $24.1\% \pm 2.4\%$ and still a warmer PL
 452 emission than the reference sample.

453 Alongside, the study concerning the influence of
 454 $R_{o/i}$ ratio on powder emission properties is presented
 455 in Fig. 4. $R_{o/i}$ ratio increases from 4 to 8 while R_o is
 456 kept at the reference value of 1.5. The PL emission
 457 spectra (Fig. 4a) are obtained with an excitation
 458 wavelength of 385 nm. Increasing the $R_{o/i}$ ratio from
 459 4 to 6.5 makes the PL emission warmer and broader.
 460 Beyond 6.5, the PL emission shifts toward the shorter

wavelengths. Therefore, the sample for which $R_{o/i}$ 461
 ratio is 6.5 generates the warmest and broadest 462
 emission band, ranging from 400 to 700 nm. 463
 Regarding the eQYs (Fig. 4b), the optimum value is 464
 for $R_{o/i} = 7$ (eQY = $22.6\% \pm 2.3\%$). However, the 465
 best compromise between a rather efficient eQY and 466
 a broad and warm PL emission is given by the $R_{o/i}$ 467
 ratio of 6.5. Indeed, this $R_{o/i}$ ratio at 6.5 provides a PL 468
 emission band significantly shifted by 50 nm toward 469
 the long wavelengths in comparison to $R_{o/i} = 7$, 470
 while maintaining an eQY of $20.3\% \pm 2.0\%$. 471

472 Considering these results, an optimized composition 473
 was chosen allowing to improve the optical 474
 characteristics (colorimetry, quantum efficiency) 475
 while maintaining a reproducible synthesis. It is 476
 characterized by the following ratios: $R_o = 1$ and $R_{o/}$
 $i = 6.5$. Thus, we can guess that the optimization of 477
 the carbonated precursors quantities has led to more 478

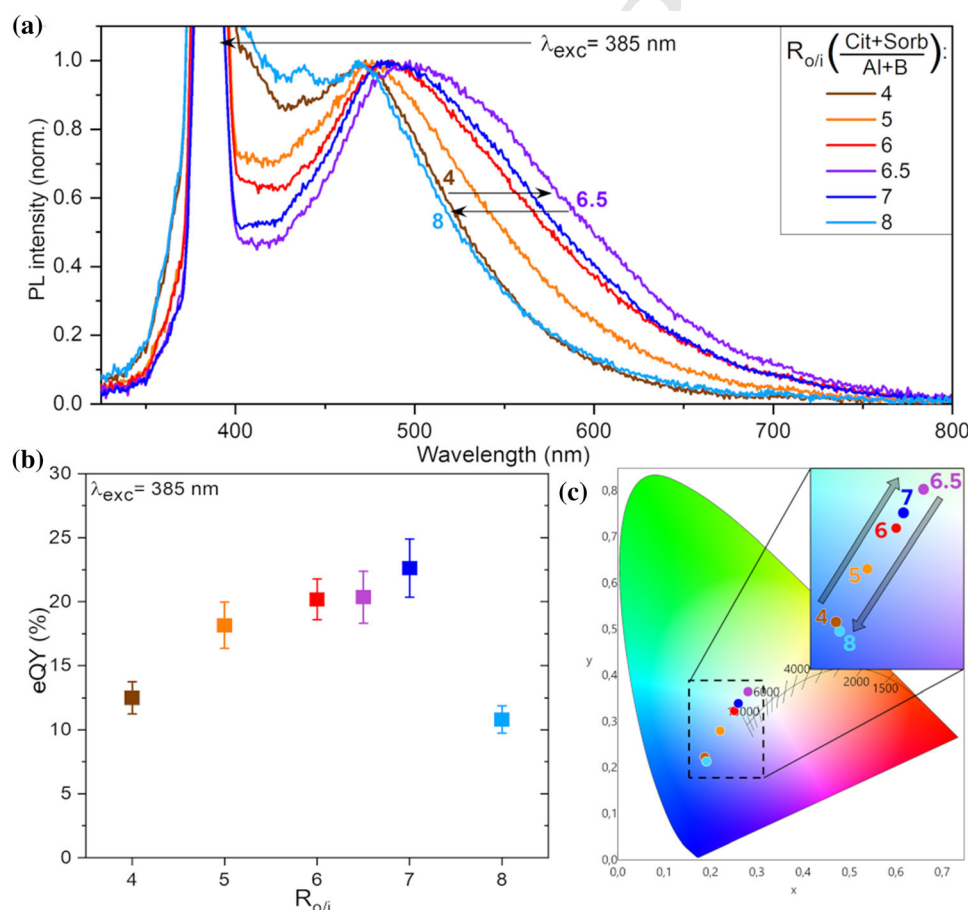


Figure 4 Normalized PL emission spectra (a) and corresponding eQYs (b) and CIE chromaticity coordinates (c) of AB samples with $R_{o/i}$ ratios varying from 4 to 8.

479 PL emitting centers (PAH molecules) trapped in the
480 aluminum borate matrix while keeping identical the
481 other synthesis conditions.

482 Optimization of the calcination parameters

483 Once the precursors composition has been optimized,
484 attention was focused on calcination parameters. This
485 thermal treatment is crucial for the PL emission
486 properties of AB powders. Thermogravimetric anal-
487 ysis coupled mass spectrometry (TGA-MS, Figure S7)
488 shows a 7 wt% loss of water between 100 and 200 °C
489 demonstrating the slight hygroscopicity of the pow-
490 der. The main mass loss of 73 wt% for the tempera-
491 ture range 450–600 °C is related to the decomposition
492 of the pyrolytic carbon eliminated by oxidation (CO₂,
493 CO and H₂O exhaust gases). In addition, this thermal
494 treatment leads to the trapping of emitting centers
495 formed within the inorganic matrix when it densifies.
496 Thus, the oxidation conditions of pyrolyzed powders
497 induce variations in the PL emission profiles and in
498 photometric characteristics of the AB powders.
499 Therefore, we optimized the calcination conditions
500 by varying the HR and the final T_{ca} around previ-
501 ously defined values (HR = 30 °C/h and
502 T_{ca} = 700 °C).

503 The HR variation keeping the same final reference
504 temperature of 700 °C was first studied. Figure 5
505 shows the results of PL emissions and eQY versus
506 HR. The three circular photographs in Fig. 5 corre-
507 spond to the calcined powders prepared with HR =
508 20, 40 and 90 °C/h. For a slow HR (20 °C/h), the
509 obtained yellowish-colored powder exhibits a narrow

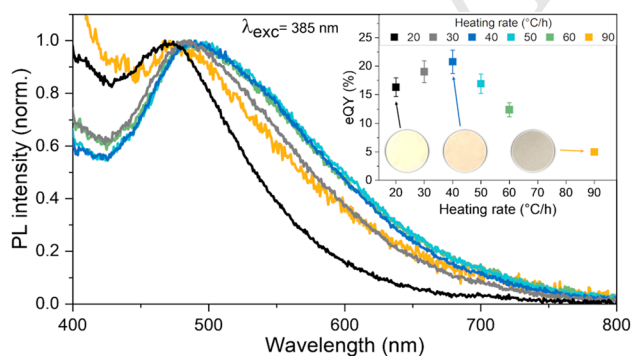


Figure 5 Normalized PL emission spectra and corresponding eQYs of AB samples calcined at different HR (from 20 °C/h to 90 °C/h) to the T_{ca} of 700 °C. Three round photographs of the powders calcined, respectively, at 20 °C/h, 40 °C/h and 90 °C/h are presented in the eQY graph.

510 PL emission in the blue range and a moderate eQY. In
511 this case, the long heating time to reach the final T_{ca}
512 (700 °C) is associated to a slow formation and den-
513 sification of the aluminum borate matrix. This favors
514 the strong oxidation of the previously pyrolyzed
515 powder. Thus, a part of the emitting centers (PAHs)
516 has been degraded by the long oxidation step, in
517 particular those emitting in the yellow range. On the
518 opposite, the powder calcined through high HR
519 (90 °C/h) has been partially oxidized exhibiting a
520 grayish color due to the significant presence of black
521 carbon. The fast heating treatment must have favored
522 the rapid densification of the AB inorganic matrix.
523 This did not allow to sufficiently oxidize a part of the
524 pyrolytic carbon, which thus remained trapped in the
525 aluminum borate network. The residual black carbon
526 species act as non-radiative absorbing centers
527 resulting in low PL efficiency (eQY = 5% ± 0.5%).
528 Intermediate HR value (40 °C/h) leads to beige
529 powder exhibiting the maximum of eQY
530 (20.8% ± 2.1%) and the widest PL emission in the
531 visible range (Fig. 5). We can therefore consider that
532 this HR corresponds to an optimized residence time
533 in the furnace, leading to the best calcination condi-
534 tions with the simultaneous formation of the AB
535 matrix and a wide range of emitting centers.

536 We adjusted the final temperature of calcination
537 T_{ca} using the optimized heating rate HR = 40 °C/h.
538 A third 2.8 wt% mass loss close to 700 °C (Figure S7)
539 is related to carbon elimination, particularly origi-
540 nated from the emitting centers trapped until then in
541 the matrix. As a consequence, we have studied AB
542 powders obtained with a T_{ca} comprised between
543 680 °C and 720 °C, taking into account that for higher
544 T_{ca} the emission intensity significantly decreases

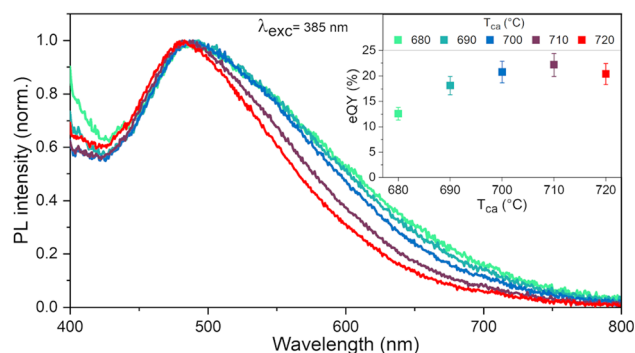


Figure 6 Normalized PL emission spectra and corresponding eQYs of AB samples calcined at different T_{ca} values from 680 °C to 720 °C with HR = 40 °C/h.

545 while the emission band shifts toward blue wave-
546 lengths. Their optical features are gathered in Fig. 6.

547 It evidences that the best compromise to get a
548 warm broad emission together with a satisfying eQY
549 is to calcine the AB sample at 700 °C. Indeed, even if
550 the eQY maximum is reached with $T_{ca} = 710$ °C, the
551 emission bandwidth is significantly reduced above
552 700 °C. Below 700 °C, the emission bandwidth is
553 almost not affected, but the eQY is quite lower indi-
554 cating a less-efficient transformation of PAH mole-
555 cules. Thus, the evolution in photometric
556 characteristics are mainly related to the one of the
557 PAH nature through partial oxidation during the
558 calcination [40] (as hydroxylated PAH) before elimi-
559 nation at higher temperature (720 °C).

560 In conclusion, the optimized calcination conditions
561 are a HR of 40 °C/h and a temperature T_{ca} of 700 °C.
562 The next part of this work will be dedicated to the use
563 of TRPL to study the origin of the PL and the dif-
564 ferences that may arise from the changes in the pre-
565 cursors ratio.

566 Time-resolved photoluminescence

567 TRPL analyses have been conducted on the opti-
568 mized AB powder (Fig. 7) and the reference sample
569 (see Table 1 for composition and Figure S9 for the
570 decays) at the excitation wavelength of 400 nm. Three
571 emission wavelengths have been studied: 448 nm for
572 the blue contribution, 506 nm corresponding to the
573 maximum of emission and 563 nm for the yellow

contribution of the emission spectrum. The data were
574 normalized and fitted with a bi-exponential decay
575 Eq. (3):
576

$$y = A_1 \exp\left(\frac{-t}{\tau_1}\right) + A_2 \exp\left(\frac{-t}{\tau_2}\right) \quad (3)$$

τ_1 and τ_2 are the short and long lifetimes, respec-
578 tively. A_1 and A_2 are the weights corresponding to
581 each part of the decay. Figure 7 shows the results
582 obtained thanks to the bi-exponential fitting for the
583 three emission wavelengths studied. The results of
584 the fit are gathered in Table 2.

The TRPL measurements of AB powders suggest
586 the presence of several types or sizes [44] of emitting
587 species as they are characterized by two decay life-
588 times. The optimized sample decay curve for the
589 448 nm emission wavelength is characterized by
590 quite equiponderant contributions of 45% and 55%,
591 respectively, for the short lifetime ($\tau_1 = 0.7 \pm 0.1$ ns)
592 and the long lifetime ($\tau_2 = 2.4 \pm 0.1$ ns). For emission
593 wavelength in the green range ($\lambda_{em} = 506$ nm), the
594 long lifetime is more weighted with 60%, and both
595 short and long time constants present increased val-
596 ues compared with the blue wavelength decay:
597 $\tau_1 = 0.9 \pm 0.1$ ns and $\tau_2 = 2.8 \pm 0.1$ ns. The trend
598 continues for the yellow emission wavelength (λ_{em} -
599 = 563 nm), with $A_1 = 30\%$ and $A_2 = 70\%$, the short
600 lifetime weight is reduced for the benefit of the long
601 lifetime. This tendency is well noticeable in Fig. 7, as
602 well as the evolution of τ_1 and τ_2 whose both values
603 increase to 1.4 ± 0.1 ns and 3.6 ± 0.1 ns, respec-
604 tively. The evolution of the values and the weights of
605 τ_1 and τ_2 with the different emission wavelengths
606 supports the hypothesis of the presence of several
607 types or sizes of PAH emitting centers.

The behavior of the decays of the reference sample
609 (Figure S9, Table 2) is very analogous to the one of the
610 optimized samples. If this similarity of the lifetimes
611 suggests that the nature of the emitting centers of the
612 reference and optimized powders are close, the
613 improvements of eQY and the broadening with
614 bathochromic effect should be attributed to the
615 quantity of emitting centers and to their fashion of
616 trapping in the inorganic matrix.

The final part of this work will highlight the tun-
618 ability of the emission features of the AB powders
619 depending on the excitation wavelength.
620

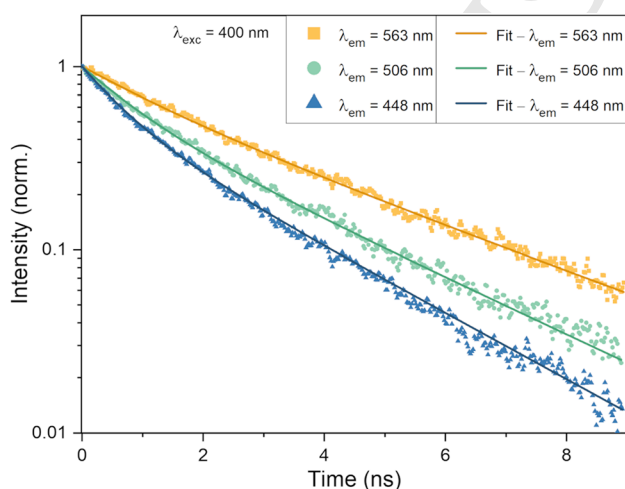
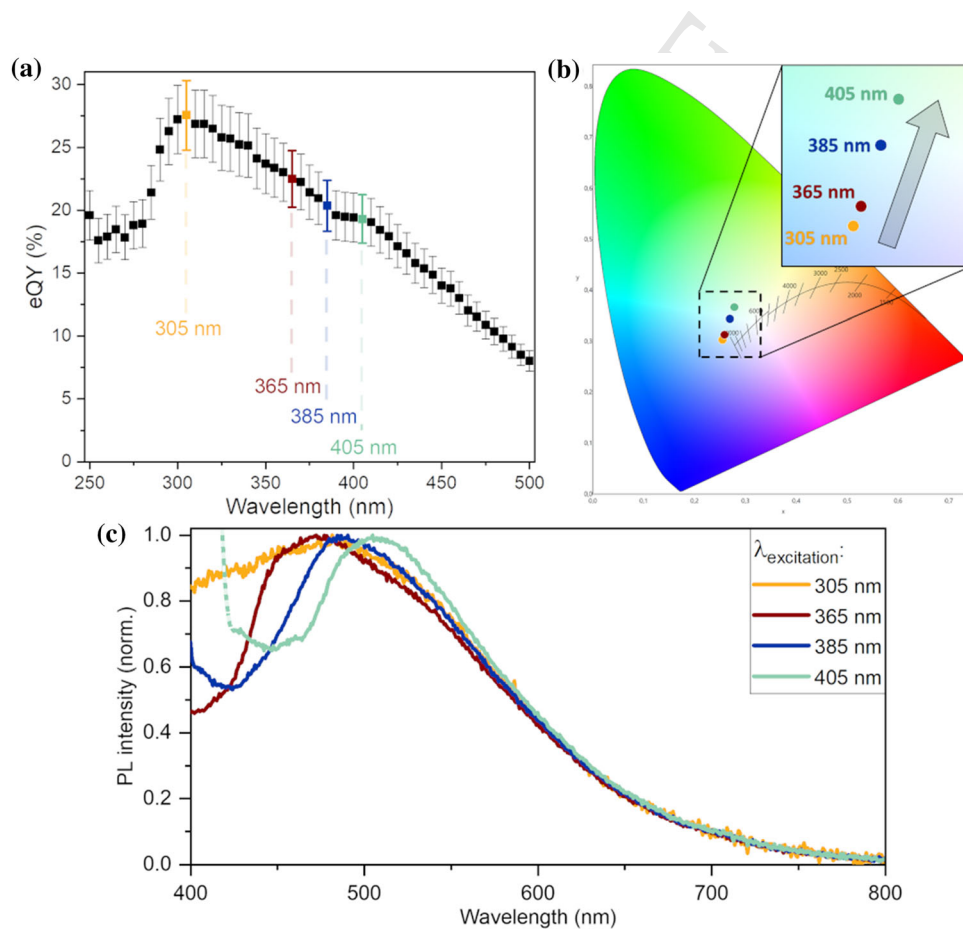


Figure 7 Room-temperature decay curves of optimized AB powder recorded under 400 nm-excitation for different emission wavelengths.

Table 2 Short and long lifetimes (τ_1 , τ_2) and associated weights (A1, A2) obtained by fitting (bi-exponential decay) the TRPL data of optimized and reference AB powders excited at 400 nm, for three emission wavelengths (448 nm, 506 nm and 563 nm)

Sample	λ_{em} (nm)	τ_1 (ns)	τ_2 (ns)	A1 (%)	A2 (%)	R ²
Optimized	448	0.7 ± 0.1	2.4 ± 0.1	45	55	0.9985
	506	0.9 ± 0.1	2.8 ± 0.1	40	60	0.9975
	563	1.4 ± 0.1	3.6 ± 0.1	30	70	0.9974
Reference	448	0.6 ± 0.1	2.4 ± 0.1	46	54	0.9980
	506	0.9 ± 0.1	2.9 ± 0.1	40	60	0.9984
	563	1.2 ± 0.1	3.6 ± 0.1	32	68	0.9965

Figure 8 eQYs (a), corresponding CIE coordinates (b) and normalized PL emission spectra (c) of optimized AB powder with focus on the maximum eQY value at 305 nm and usual near-UV chip wavelengths at 365, 385 and 405 nm..

621 Excitation wavelength modulation

622 The AB luminescent powders offer a particularly
 623 interesting characteristic: they can be excited in a
 624 wide range of wavelengths from UV to blue wave-
 625 lengths as illustrated for the optimized powder in
 626 Fig. 8a. Thus, the most-used commercial UV wave-
 627 lengths (365 nm, 385 nm, 405 nm) are included in
 628 this excitation domain. The maximum eQY is
 629 $27.6\% \pm 2.8\%$ for $\lambda_{exc} = 305$ nm. The corresponding
 630 PL emission spectrum and those measured with

631 $\lambda_{exc} = 365$ nm, 385 nm and 405 nm are presented in
 632 Fig. 8c. The associated CIE chromaticity coordinates
 633 (Fig. 8b) highlight the bathochromic emission shift
 634 occurring for the same sample when the excitation
 635 wavelength increases.

636 This tunable emission profile could be explained
 637 by the existence of PAHs of different sizes, such as
 638 coronene or circumcoronene molecules as recently
 639 evidenced by Salaün et al. combining spectroscopic
 640 results (PL, EPR) and DFT calculations [40]. This
 641 specific behavior is particularly interesting for tuning

642 the white emission from pretty cold to pretty warm
643 color, including AB powders in a device combining
644 different kinds of UV-LEDs.

645 Conclusion

646 In this work, RE-free AB phosphors presenting a
647 broad PL emission band in the visible range under
648 near-UV excitation have been developed by a modi-
649 fied Pechini process. Their PL properties are due to
650 the presence of PAH emitting centers trapped in the
651 inorganic matrix. The different steps of the synthesis
652 have been optimized to improve the photometric
653 properties of AB powders. Both inorganic and
654 organic precursors molar ratios were optimized.
655 Respectively, $A1/B = 0.5$, $Cit/Sorb = 1$ and $(Cit +$
656 $Sorb)/(A1 + B) = 6.5$ are the ratios for which PL
657 emission is the widest and warmest (from 400 to
658 700 nm) with near-UV excitation (385 nm). The
659 trapping properties of the inorganic AB matrix were
660 enhanced, while the formation of PAH molecules
661 emitting at warmer wavelengths was promoted.
662 Then, the parameters of the calcination treatment,
663 under O_2 atmosphere, were adjusted. During this last
664 synthesis step, the oxidation of organic residues
665 resulting from the previous pyrolysis and acting as
666 absorbing centers, is completed. The best conditions
667 allowing a suitable oxidation step leading to the
668 formation and conservation of emitting centers were
669 determined: a heating rate of $40\text{ }^\circ\text{C/h}$ and a calcina-
670 tion temperature of $700\text{ }^\circ\text{C}$. TRPL measurements
671 were performed to characterize the PAH emitting
672 centers in the solid state. The optimized powder
673 presents a satisfying eQY from 19 to 28% on a wide
674 range of UV-excitation wavelengths (from 305 to
675 405 nm). Moreover, the possibility of adapting the
676 excitation wavelength to get an emission band with
677 controlled profile has been described. It is quite
678 interesting for applications in which the color of
679 emission needs to be tuned in a condensed device
680 with a single phosphor associated to several UV-ex-
681 citation sources.

682 Acknowledgment

683 The authors thank Christelle Blavignac (Centre Ima-
684 gerie Cellulaire Santé – Université Clermont

Auvergne, France) for her technical support for TEM 685
observations. 686

Funding

This work was carried out under Région Auvergne 688
Rhône Alpes, Pack Ambition Recherche 2019, 689
“LUMINOLED” project. 690

Declarations

Conflict of interest The authors declare that they 692
have no conflict of interest. 693

Supplementary Information: The online version 694
contains supplementary material available at [http](http://doi.org/10.1007/s10853-022-07619-5) 695
[://doi.org/10.1007/s10853-022-07619-5](http://doi.org/10.1007/s10853-022-07619-5). 696

References

- [1] Nair GB, Swart HC, Dhoble SJ (2020) A review on the 698
advancements in phosphor-converted light emitting diodes 699
(pc-LEDs): Phosphor synthesis, device fabrication and 700
characterization. *Prog Mater Sci* 109:100622. [https://doi.org/](https://doi.org/10.1016/j.pmatsci.2019.100622) 701
[10.1016/j.pmatsci.2019.100622](https://doi.org/10.1016/j.pmatsci.2019.100622) 702
- [2] Yang L, Chen M, Lv Z et al (2013) Preparation of a YAG: Ce 703
phosphor glass by screen-printing technology and its appli- 704
cation in LED packaging. *Opt Lett* 38:2240. [https://doi.org/](https://doi.org/10.1364/OL.38.002240) 705
[10.1364/OL.38.002240](https://doi.org/10.1364/OL.38.002240) 706
- [3] Cho J, Park JH, Kim JK, Schubert EF (2017) White light- 707
emitting diodes: History, progress, and future: White light- 708
emitting diodes. *Laser Photon Rev* 11:1600147. [https://doi.](https://doi.org/10.1002/lpor.201600147) 709
[org/10.1002/lpor.201600147](https://doi.org/10.1002/lpor.201600147) 710
- [4] Ye S, Xiao F, Pan YX et al (2010) Phosphors in phosphor- 711
converted white light-emitting diodes: recent advances in 712
materials, techniques and properties. *Mater Sci Eng R Rep* 713
71:1–34. <https://doi.org/10.1016/j.mser.2010.07.001> 714
- [5] Hu Y, Zhuang W, Ye H et al (2005) Preparation and lumi- 715
nescent properties of (Ca1-x, Srx)S:Eu2+ red-emitting 716
phosphor for white LED. *J Lumin* 111:139–145. [https://doi.](https://doi.org/10.1016/j.jlumin.2004.07.005) 717
[org/10.1016/j.jlumin.2004.07.005](https://doi.org/10.1016/j.jlumin.2004.07.005) 718
- [6] Pricha I, Rossner W, Moos R (2016) Layered ceramic 719
phosphors based on $CaAlSiN_3$: Eu and YAG: Ce for white 720
light-emitting diodes. *J Am Ceram Soc* 99:211–217. [https://d](https://doi.org/10.1111/jace.13948) 721
[oi.org/10.1111/jace.13948](https://doi.org/10.1111/jace.13948) 722
- [7] Jargus V, Nedoma, et al (2019) Effect of selected lumines- 723
cent layers on CCT, CRI, and response times. *Materials* 724
12:2095. <https://doi.org/10.3390/ma12132095> 725

- 726 [8] Fukui T, Kamon K, Takeshita J et al (2009) Superior illu- 775
 727 minant characteristics of color rendering and luminous effi- 776
 728 cacy in multilayered phosphor conversion white light 777
 729 sources excited by near-ultraviolet light-emitting diodes. Jpn 778
 730 J Appl Phys 48:112101. [https://doi.org/10.1143/JJAP.48.](https://doi.org/10.1143/JJAP.48.112101) 779
 731 [112101](https://doi.org/10.1143/JJAP.48.112101) 780
- 732 [9] Li R, Li H, Peng Y, et al (2016) Development of RGB 781
 733 phosphor-in-glass for ultraviolet-excited white light-emitting 782
 734 diodes packaging. In: 2016 17th International Conference on 783
 735 Electronic Packaging Technology (ICEPT). IEEE, Wuhan, 784
 736 China, pp 94–97 785
- 737 [10] Peng Y, Cheng H, Chen Z, Li R (2016) Multi-layered Red, 786
 738 Green, and Blue Phosphor-in- Glass for Ultraviolet-Excited 787
 739 White Light-Emitting Diodes Packaging. Th Int Conf Elec- 788
 740 tron Packag Technol 4 789
- 741 [11] Shang M, Li C, Lin J (2014) How to produce white light in a 790
 742 single-phase host? Chem Soc Rev 43:1372–1386. [https://doi.](https://doi.org/10.1039/C3CS60314H) 791
 743 [org/10.1039/C3CS60314H](https://doi.org/10.1039/C3CS60314H) 792
- 744 [12] Smet PF, Parmentier AB, Poelman D (2011) Selecting con- 793
 745 version phosphors for white light-emitting diodes. J Elec- 794
 746 trochem Soc 158:R37. <https://doi.org/10.1149/1.3568524> 795
- 747 [13] Bachmann V, Ronda C, Meijerink A (2009) Temperature 796
 748 quenching of yellow Ce³⁺ luminescence in YAG:Ce. Chem 797
 749 Mater 21:2077–2084. <https://doi.org/10.1021/cm8030768> 798
- 750 [14] Ivanovskikh KV, Ogiegło JM, Zych A et al (2013) Lumi- 799
 751 nescence temperature quenching for Ce³⁺ and Pr³⁺ *d-f* 800
 752 emission in YAG and LuAG. ECS J Solid State Sci Technol 801
 753 2:R3148–R3152. <https://doi.org/10.1149/2.011302jss> 802
- 754 [15] European Commission (2016) Critical raw materials. In: 803
 755 Intern. Mark. Ind. Entrep. SMEs - Eur. Comm. [https://ec.e](https://ec.europa.eu/growth/sectors/raw-materials/specific-interest/critical_en) 804
 756 [uropa.eu/growth/sectors/raw-materials/specific-interest/critic](https://ec.europa.eu/growth/sectors/raw-materials/specific-interest/critical_en) 805
 757 [al_en](https://ec.europa.eu/growth/sectors/raw-materials/specific-interest/critical_en). Accessed 13 Apr 2022 806
- 758 [16] Golev A, Scott M, Erskine PD et al (2014) Rare earths 807
 759 supply chains: Current status, constraints and opportunities. 808
 760 Resour Policy 41:52–59. [https://doi.org/10.1016/j.resourpol.](https://doi.org/10.1016/j.resourpol.2014.03.004) 809
 761 [2014.03.004](https://doi.org/10.1016/j.resourpol.2014.03.004) 810
- 762 [17] Ali S (2014) Social and environmental impact of the rare 811
 763 earth industries. Resources 3:123–134. [https://doi.org/10.33](https://doi.org/10.3390/resources3010123) 812
 764 [90/resources3010123](https://doi.org/10.3390/resources3010123) 813
- 765 [18] Binnemans K, Jones PT, Blanpain B et al (2013) Recycling 814
 766 of rare earths: a critical review. J Clean Prod 51:1–22. <https://doi.org/10.1016/j.jclepro.2012.12.037> 815
 767 <https://doi.org/10.1016/j.jclepro.2012.12.037> 816
- 768 [19] Rare Earths Statistics and Information. [https://www.usgs.g](https://www.usgs.gov/centers/nmic/rare-earths-statistics-and-information) 817
 769 [ov/centers/nmic/rare-earths-statistics-and-information](https://www.usgs.gov/centers/nmic/rare-earths-statistics-and-information). 818
 770 Accessed 13 Apr 2022 819
- 771 [20] (2020) How Rare-Earth Mining Has Devastated China's 820
 772 Environment. In: EarthOrg - Past Present Future. [https://ea](https://earth.org/rare-earth-mining-has-devastated-chinas-environment/) 821
 773 [rth.org/rare-earth-mining-has-devastated-chinas-environmen](https://earth.org/rare-earth-mining-has-devastated-chinas-environment/) 822
 774 [t/](https://earth.org/rare-earth-mining-has-devastated-chinas-environment/). Accessed 13 Apr 2022 823
- [21] Liang T, Li K, Wang L (2014) State of rare earth elements in 775
 different environmental components in mining areas of 776
 China. Environ Monit Assess 186:1499–1513. [https://doi.](https://doi.org/10.1007/s10661-013-3469-8) 777
[org/10.1007/s10661-013-3469-8](https://doi.org/10.1007/s10661-013-3469-8) 778
- [22] Pan Y, Li H (2016) Investigating heavy metal pollution in 779
 mining brownfield and its policy implications: a case study 780
 of the Bayan Obo rare Earth Mine, Inner Mongolia, China. 781
 Environ Manage 57:879–893. [https://doi.org/10.1007/s0026](https://doi.org/10.1007/s00267-016-0658-6) 782
[7-016-0658-6](https://doi.org/10.1007/s00267-016-0658-6) 783
- [23] Duan CJ, Delsing ACA, Hintzen HT (2009) Photolumines- 784
 cence properties of novel red-emitting Mn²⁺-Activated 785
 MZnOS (M = Ca, Ba) phosphors. Chem Mater 21:1010–1016. <https://doi.org/10.1021/cm801990r> 786
<https://doi.org/10.1021/cm801990r> 787
- [24] Chen D (2016) A review on Mn⁴⁺ activators in solids for 788
 warm white light-emitting diodes. RSC Adv 12 789
- [25] Kumar V, Potdevin A, Boutinaud P, Boyer D (2020) HF-free 790
 synthesis of K₂SiF₆ and BaSiF₆ nanoparticles by thermal 791
 decomposition. Mater Lett 261:127123. [https://doi.org/10.1](https://doi.org/10.1016/j.matlet.2019.127123) 792
[016/j.matlet.2019.127123](https://doi.org/10.1016/j.matlet.2019.127123) 793
- [26] Kurtin J (2013) Quantum dot LED phosphors: performance 794
 and reliability improvements. In: Streubel KP, Jeon H, Tu 795
 L-W, Strassburg M (eds) San Francisco. California, USA, 796
 p 86411D 797
- [27] Wang J, Yang Y, Liu X (2020) Solid-state fluorescent carbon 798
 dots: quenching resistance strategies, high quantum effi- 799
 ciency control, multicolor tuning, and applications. Mater 800
 Adv 1:3122–3142. <https://doi.org/10.1039/D0MA00632G> 801
<https://doi.org/10.1039/D0MA00632G> 802
- [28] Guo X, Wang C-F, Yu Z-Y et al (2012) Facile access to 803
 versatile fluorescent carbon dots toward light-emitting 804
 diodes. Chem Commun 48:2692. [https://doi.org/10.1039/c](https://doi.org/10.1039/c2cc17769b) 805
[2cc17769b](https://doi.org/10.1039/c2cc17769b) 806
- [29] Zhu J, Shao H, Bai X et al (2018) Modulation of the pho- 806
 toluminescence in carbon dots through surface modification: 807
 from mechanism to white light-emitting diodes. Nanotech- 808
 nology 29:245702. [https://doi.org/10.1088/1361-6528/aab9d](https://doi.org/10.1088/1361-6528/aab9d6) 809
[6](https://doi.org/10.1088/1361-6528/aab9d6) 810
- [30] Xie Z, Yin Z, Wu Y et al (2017) White light-emitting diodes 811
 based on individual polymerized carbon nanodots. Sci Rep 812
 7:12146. <https://doi.org/10.1038/s41598-017-12083-2> 813
<https://doi.org/10.1038/s41598-017-12083-2> 814
- [31] Zhu J, Bai X, Zhai Y et al (2017) Carbon dots with efficient 814
 solid-state photoluminescence towards white light-emitting 815
 diodes. J Mater Chem C 5:11416–11420. [https://doi.org/10.](https://doi.org/10.1039/C7TC04155A) 816
[1039/C7TC04155A](https://doi.org/10.1039/C7TC04155A) 817
- [32] Onal A, Eren GO, Sadeghi S et al (2022) High-performance 818
 white light-emitting diodes over 150 lm/W using near-unity- 819
 emitting quantum dots in a liquid matrix. ACS Photon 820
 Acsphoton. <https://doi.org/10.1021/acsphotonics.1c01805> 821
<https://doi.org/10.1021/acsphotonics.1c01805> 822
- [33] Green WH (1997) White phosphors from a silicate-car- 822
 boxylate sol-gel precursor that lack metal activator ions. 823

- 824 Science 276:1826–1828. <https://doi.org/10.1126/science.276.5320.1826>
- 825
- 826 [34] Davies G-L, McCarthy JE, Rakovich A, Gun'ko YK (2012)
- 827 Towards white luminophores: developing luminescent silica
- 828 on the nanoscale. *J Mater Chem* 22:7358. <https://doi.org/10.1039/c2jm16086b>
- 829
- 830 [35] Hayakawa T, Hiramitsu A, Nogami M (2003) White light
- 831 emission from radical carbonyl-terminations in Al₂O₃–SiO₂
- 832 porous glasses with high luminescence quantum efficiencies.
- 833 *Appl Phys Lett* 82:2975–2977. <https://doi.org/10.1063/1.1569038>
- 834
- 835 [36] Guimarães VF, Maia LJQ, Gautier-Luneau I et al (2015)
- 836 Toward a new generation of white phosphors for solid state
- 837 lighting using glassy yttrium aluminoborates. *J Mater Chem*
- 838 *C* 3:5795–5802
- 839 [37] Burner P, Sontakke AD, Salaün M et al (2017) Evidence of
- 840 organic luminescent centers in Sol–Gel-synthesized yttrium
- 841 aluminum borate matrix leading to bright visible emission.
- 842 *Angew Chem Int Ed* 56:13995–13998. <https://doi.org/10.1002/anie.201706070>
- 843
- 844 [38] Sontakke AD, Ferrier A, Burner P et al (2017) Afterglow
- 845 luminescence in wet-chemically synthesized inorganic
- 846 materials: ultra-long room temperature phosphorescence
- 847 instead of persistent luminescence. *J Phys Chem Lett*
- 848 8:4735–4739. <https://doi.org/10.1021/acs.jpcclett.7b01702>
- 849 [39] Sontakke AD, Mouesca J-M, Castaing V et al (2018) Time-
- 850 gated triplet-state optical spectroscopy to decipher organic
- 851 luminophores embedded in rigid matrices. *Phys Chem Chem*
- 852 *Phys* 20:23294–23300. <https://doi.org/10.1039/C8CP03952F>
- 853
- [40] Salaün M, Sontakke AD, Maurel V et al (2022) Relation between material structure and photoluminescence properties in yttrium–aluminum borates phosphors. *MRS Bull* 47:231–242. <https://doi.org/10.1557/s43577-021-00195-0>
- [41] Gaffuri P, Salaün M, Gautier-Luneau I et al (2020) Rare-earth-free zinc aluminium borate white phosphors for LED lighting. *J Mater Chem C* 8:11839–11849. <https://doi.org/10.1039/D0TC02196B>
- [42] Mutailipu M, Poeppelmeier KR, Pan S (2021) Borates: a rich source for optical materials. *Chem Rev* 121:1130–1202. <https://doi.org/10.1021/acs.chemrev.0c00796>
- [43] Guimarães VF, Salaün M, Burner P et al (2017) Controlled preparation of aluminum borate powders for the development of defect-related phosphors for warm white LED lighting. *Solid State Sci* 65:6–14. <https://doi.org/10.1016/j.solidstatesciences.2016.12.011>
- [44] Ehrat F, Bhattacharyya S, Schneider J et al (2017) Tracking the source of carbon dot photoluminescence: aromatic domains versus molecular fluorophores. *Nano Lett* 17:7710–7716. <https://doi.org/10.1021/acs.nanolett.7b03863>

Publisher's Note Springer Nature remains neutral with regard to jurisdictional claims in published maps and institutional affiliations.

Springer Nature or its licensor holds exclusive rights to this article under a publishing agreement with the author(s) or other rightsholder(s); author self-archiving of the accepted manuscript version of this article is solely governed by the terms of such publishing agreement and applicable law.